V International Conference on Particle-based Methods – Fundamentals and Applications
PARTICLES 2017
P. Wriggers, M. Bischoff, E. Oñate, D.R.J. Owen, & T. Zohdi (Eds)

MOVING PARTICLE SIMULATION WITH SOLID-SOLID CONTACT

RUBENS A. AMARO JUNIOR, PEDRO H. S. OSELLO AND LIANG-YEE CHENG

Department of Construction Engineering (PCC)
Polytechnic School of University of São Paulo (EPUSP)
Cidade Universitária, 05508-070 São Paulo, Brazil
rubens.amaro@usp.br, http://www.pcc.usp.br/home/

Key words: Solid-solid contact, rigid body dynamics, MPS, Moving particle simulation.

Abstract. Problems of fluid-structure interaction with free surface flow and multi-body interactions are highly nonlinear and complex phenomena, which is challenging for computational modeling and simulation. In the presence of contact or collision between solids, numerical modeling to detect collision and prevent penetration between bodies is required. The objective of this work is to study a numerical model for solid-solid contact and/or collision, based on contact mechanics theories, to reproduce the macroscopic properties of the multi-body interactions in Moving Particle Simulation (MPS) method. MPS is a fully Lagrangian meshfree particle-based approach that is suitable for the modeling complex geometries with large displacements and deformation, including free surface flow with fragmentation and merging and interaction of fluid with multi-bodies. Analytical results are used to perform the calibration of the numerical friction coefficient. The model is applied to a case of free solid transport in free surface flow, modeled as a 3D experimental dam breaking event, in which free solids interact each other and fixed walls. The numerical results from MPS are compared with numerical and experimental results.

1 INTRODUCTION

Fluid-structure interaction with free surface flow and multi-body interactions, are highly nonlinear and complex hydrodynamic phenomena, which is challenging problems for computational modeling and simulation. Among the effective numerical methods used to simulate these phenomena an important approach is the particle-based method, in which the physical domain is represented by a set of points (particles). However, despite the easier implementation and flexibility of these methods, one of the relevant topics is concerning the numerical treatment of contacts between bodies when contact or collision between solids occurs. To date, different techniques have been proposed for particle methods to deal with the contact between solids, such as impulse-based repulsion models [1,2] and linear [3,4,5] or nonlinear [6] springs and dashpots. Based on contact mechanics theories, the objective of this work is to study a nonlinear spring and dashpot model of solid-solid contact and/or collision for Moving Particle Simulation (MPS) method [7]. MPS is a fully Lagrangian meshfree particle-based approach suitable for the modeling of complex geometries with large displacements and deformation, including free surface flow with fragmentation and coalescence and interaction of fluid with multi-bodies. The relationship between the numerical and analytical friction coefficient is investigated by a case of block's sliding along

a slope, subjected to gravity acceleration. For the validation, a 3D experimental dam breaking event, in which free cubic solids interact each other and fixed walls [6], is simulated. Numerical results of solid position obtained by the proposed model are compared with available numerical and experimental results.

2 NUMERICAL METHOD

In MPS method, the differential operators of the governing equations of continuum are replaced by operators based on a weight function. For a given particle i, the influence of a neighbor particle j is defined by weight function ω_{ij}

$$\omega_{ij} = \begin{cases} \frac{r_e}{\|\vec{r}_{ij}\|} - 1 & \|\vec{r}_{ij}\| \leq r_e \\ 0 & \|\vec{r}_{ij}\| > r_e \end{cases}, \tag{1}$$

where r_e is the effective radius that limits the range of influence and $\|\vec{r}_{ij}\|$ is the distance between i and j. In the present work, is used the effective radius $r_e = 2.1 l_0$, where l_0 is the initial distance between two adjacent particles.

The summation of the weight of all the particles in the neighborhood of the particle i is defined as its particle number density n_i, which is proportional to the fluid density

$$n_i = \sum_{j \neq i} \omega_{ij}. \tag{2}$$

For a scalar function ϕ, the gradient and Laplacian operators are defined in Eq. 3 and Eq. 4, respectively

$$\nabla \phi = \frac{d}{n^0} \sum_{j \neq i} \frac{\phi_j - \phi_i}{\|\vec{r}_{ij}\|^2} \vec{r}_{ij} \omega_{ij}, \tag{3}$$

$$\nabla^2 \phi = \frac{2d}{\lambda_i n^0} \sum_{j \neq i} (\phi_j - \phi_i) \omega_{ij}, \tag{4}$$

where d is the number of spatial dimensions and n^0 is the initial value of n_i. Finally, λ_i is a correction parameter so that the variance increase is equal to that of the analytical solution, and is calculated by

$$\lambda_i = \frac{\sum_{j \neq i} \omega_{ij} \|\vec{r}_{ij}\|^2}{\sum_{j \neq i} \omega_{ij}}. \tag{5}$$

2.1 Fluid dynamics

The governing equations of incompressible viscous flow are expressed by the conservation laws of mass and momentum:

$$\frac{D\rho}{Dt} = \rho \nabla \cdot \vec{u} = 0, \tag{6}$$

$$\frac{D\vec{u}}{Dt} = -\frac{\nabla P}{\rho} + \nu\nabla^2\vec{u} + \vec{f}, \tag{7}$$

where ρ is the fluid density, $\vec{u}$ is the velocity vector, P is the pressure, ν is the kinematic viscosity and $\vec{f}$ is the external force vector.

To solve the incompressible viscous flow, a semi-implicit algorithm is used in the MPS method. At first, predictions of the particle's velocity and position are carried out explicitly by using viscosity and external forces terms of the momentum conservation. Then the pressure of all particles is calculated by the Poisson equation for the pressure as follows

$$\nabla^2 P_i^{t+\Delta t} - \frac{\rho}{\Delta t^2}\alpha P_i^{t+\Delta t} = -\gamma\frac{\rho}{\Delta t^2}\frac{n_i^* - n^0}{n^0}, \tag{8}$$

where Δt is the time step, n_i^* is the particle number density calculated based on the displacement of particles obtained in the prediction step, α is the coefficient of artificial compressibility and γ is the relaxation coefficient. Both α and γ are used to improve the stability of a computation method. Also, to provide the stabilization of MPS, the pressure gradient is modified as [7]

$$\nabla P = \frac{d}{n^0}\sum_{j\neq i}\frac{P_j - \hat{P}_i}{\|\vec{r}_{ij}\|^2}\vec{r}_{ij}\omega_{ij}, \tag{9}$$

where $\hat{P}_i$ is the minimum pressure between the neighborhood of the particle i.

Finally, the velocity of the particles is updated by using the pressure gradient term of the momentum conservation and the new positions of the particles are obtained. Validations of the present numerical method (MPS) can be found in previous works. To mention few, we have: The pressure variations inside a tank structure caused by sloshing [8]. Computed pressures on the block and free surface elevation of three-dimensional dam break problem [9]. Displacement of the elastic plate interacting with dam breaking and sloshing [10].

2.2 Boundary conditions

In order to identify the free-surface boundary, the present work used the particle number density condition [7] and the neighborhood particles weighted geometric center deviation condition [11]. A particle is defined as free-surface particle and its pressure is set to zero when its particle number density particle number density n_i is smaller than $\beta_1 n^0$, and the magnitude of the weighted average deviation σ_i is greater than $\delta_1 l_0$.

Solid wall boundary condition is imposed by using three layers of fixed particles. The particles that form the layer in contact to the fluid are denominated wall particles, of which the pressure is computed by solving Poisson equation for the pressure (Eq. 8), together with the fluid particles. The particles that form two other layers are denominated dummy particles. Dummy particles are used to assure the correct calculation of the particle number density of the wall particles. Pressure is not calculated in the dummy particles.

2.3 Rigid body dynamics

For the rigid body dynamics, the governing equations of motion are those of translational motion and rotational motion expressed as

$$m\vec{a} = \sum \vec{f}_{ext}, \tag{10}$$

$$\vec{I} \cdot \dot{\vec{\omega}} + \vec{\omega} \times (\vec{I} \cdot \vec{\omega}) = \sum \vec{M}_{ext}, \tag{11}$$

where m is the total mass of the rigid body, $\vec{a}$ is the acceleration vector at the center of the rigid body, $\vec{f}_{ext}$ is external forces, $\vec{I}$ is the inertia matrix, $\vec{\omega}$ is the angular velocity about the principal axes of the rigid body and $\vec{M}_{ext}$ is the external moment. The rigid body is discretized by a finite number of particles whose relative positions remain unchanged during the simulation. The external forces are calculated considering the effect of gravity $\vec{f}_g$, hydrodynamic forces on the rigid surface $\vec{f}_h$ and contact forces between the rigid bodies $\vec{f}_c$. The contribution of hydrodynamic added to gravity force and moment $\vec{M}$ acting on the rigid body are calculated as

$$\vec{f}_h + \vec{f}_g = -\iint_S P d\vec{s} + m\vec{g}, \tag{12}$$

$$\vec{M} = -\iint_S \vec{r} \times P d\vec{s}, \tag{13}$$

where the vector $\vec{r}$ denotes the position vector from the center of the rigid body and $d\vec{s}$ is the area multiplied by the normal vector on the rigid body surface. Focusing the impulsive hydrodynamic loads on the rigid solid, shear forces were neglected in Eq. 12 and only the normal force due pressure was considered.

The contact/collision force between the rigid bodies $\vec{f}_c$ is decomposed into normal $\vec{f}_n$ and tangential $\vec{f}_s$ components. Both forces are modeled by using a penalty-based spring dashpot model inspired by the Discrete Element Modelling (DEM) formulation [12]. They are decomposed into a repulsion force $\vec{f}^r$, proportional to the penetration between particles, and a damping force $\vec{f}^d$, representing the energy dissipation during the deformation.

The normal forces between a pair of particles ij are described following a non-linear Hertz's elastic contact theory [13]:

$$\vec{f}_{n,ij} = \vec{f}^r_{n,ij} + \vec{f}^d_{n,ij} = k_{n,ij}\delta_{ij}^{3/2}\vec{n}_c - c_{n,ij}\delta_{ij}^{1/4}\dot{\delta}_{ij}\vec{n}_c, \tag{14}$$

where $k_{n,ij}$ is the stiffness constant of pair ij, $\delta_{ij} = l_0 - \|\vec{r}_{ij}\|$ is the particle overlap (penetration), $\dot{\delta}_{ij} = (\vec{u}_j - \vec{u}_i) \cdot \vec{n}_c$ is the rate of penetration, $c_{n,ij}$ is the damping constant and $\vec{n}_c$ is the contact/collision normal vector.

The stiffness constant and damping constant are given by

$$k_{n,ij} = \frac{4}{3}E_{ij}\sqrt{l_{0,ij}}, \quad c_{n,ij} = C_n\sqrt{6m_{ij}E_{ij}\sqrt{l_{0,ij}}}, \tag{15}$$

where C_n is the ratio of the collision (which must be specified) and E_{ij}, m_{ij} and $l_{0,ij}$ are obtained as

$$E_{ij} = \frac{E_i E_j}{(1-\nu_j)E_i + (1-\nu_i)E_j}, \quad m_{ij} = \frac{m_i m_j}{m_i + m_j}, \quad l_{0,ij} = \frac{l_{0,i} l_{0,j}}{l_{0,i} + l_{0,j}}, \tag{16}$$

with E_i, E_j; and ν_i, ν_j as the Young's modulus and the Poisson's ratio of particles i and j, respectively. In the present work, only one resolution l_0 is used for all domain, thus leading to $l_{0,ij} = l_0/2$. In case j is a particle belonging to a fixed rigid wall, $m_j \to \infty$, implying that $m_{ij} = m_i$.

Tangential forces are given by a linear dash-pot following by the Coulomb friction law or repulsive and damped forces by assuming a linear model. The Coulomb law is modified with a sigmoidal function in order to make it continuous at the origin regarding the tangential velocity [14]:

$$\vec{f}_{t,ij} = \min\left(\mu_j \left\|\vec{f}_n\right\| \tanh\left(8\dot{\delta}_{ij}^t\right)\vec{t}_c, k_{t,ij}\delta_{ij}^t\vec{t}_c - c_{t,ij}\dot{\delta}_{ij}^t\vec{t}_c,\right). \tag{17}$$

Here, μ_j is the kinetic friction coefficient for the pair of particles i and j, δ_{ij}^t is the tangential deformation, $\dot{\delta}_{ij}^t$ is the rate of tangential deformation, $\vec{t}_c$ is the tangential contact/collision vector and $k_{t,ij}$ stiffness and $c_{t,ij}$ damping constants [15].

After calculation all contacts between particles, the contact forces for each rigid body is given by

$$\vec{f}_n = \frac{1}{Nc}\sum_{j=1}^{Nc}\vec{f}_{n,ij}^r + \vec{f}_{n,ij}^d, \quad \vec{f}_t = \frac{1}{Nc}\sum_{j=1}^{Nc}\vec{f}_{t,ij} \tag{18}$$

where Nc is the number of particles that are in contact with particle i.

2.4 Contact/collision normal vector

The contact/collision normal vector $\vec{n}_c$ is computed from the particle features at the moment just before the collision. A feature can be a vertex, an edge or a face of the rigid body. In the present work, the geometry of rectangular parallelepiped is enough to model all rigid bodies, therefore the number of neighbor particles are used to identify the features of a particle i.

During the simulations, the contact/collision normal vector between a pair of particles i and j is defined by:

1. Particle i or j is face, the unit vector parallel to the face normal is used as $\vec{n}_c$.
2. Neither particles are face, the unit vector distance between particles is used as $\vec{n}_c$.

The direction of $\vec{n}_c$ is chosen such that the relative velocity of the rigid bodies at the collision point along the collision normal is negative, indicating that the bodies are moving towards each other [16].

3 RESULTS AND DISCUSSIONS

3.1 Contact friction model

In order to verify the present friction model, a simple case of a free solid sliding on a sloped surface was simulated. The free solid is modeled as a rectangular cuboid with a squared base (0.2 x 0.2 x 0.1 m³) and the surface is modeled as an inclined plane of length 10.2 m and the angle of 30 degrees with horizontal, as shown in Figure 1. The free solid has no initial velocity and only gravitational and friction forces act on its motion. The numerical parameters and material properties are given in Table 1.

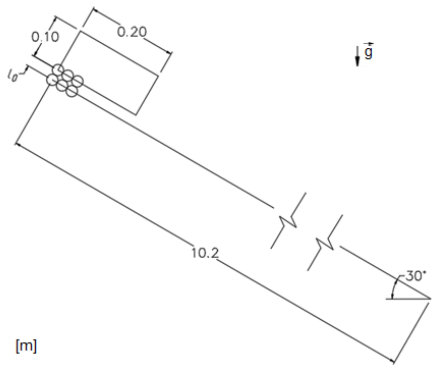

Figure 1: Main dimensions of the sloped surface and the sliding body.

Table 1: Sliding body. Numerical parameters and material properties.

Solid	*lo* (m)	*L/lo*	*ρ* (kg/m3)	*m* (kg)	*v*	*E* (MPa)	C_n (kg/s)
Body	0.025	8	780	3.12	0.3	50	1
Plane		-	∞	∞	0.3	50	-/-

Four cases with different numerical friction coefficients ($\mu_{num} = 0.15, 0.25, 0.35, 0.45$) were simulated and the equivalent analytical friction coefficient μ_{ana} were obtained by the computed accelerations of the free solid. The evolution of the body's position for both analytical and numerical results and the relation between the numerical and analytical friction coefficients are illustrated in Figure 2 (a) and Figure 2 (b), respectively. The computed positions of the free solid are very close to the analytical ones, although the numerical friction coefficients are related to the analytical ones by a factor of 1.22.

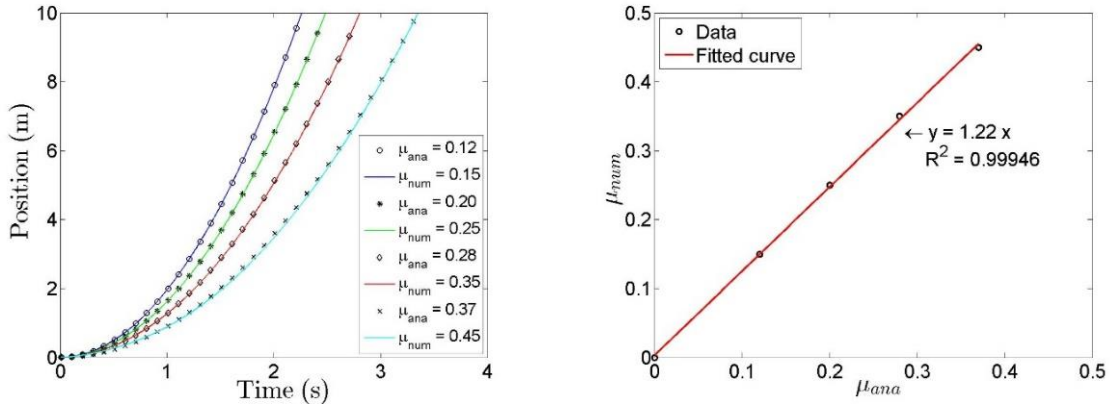

(a) (b)

Figure 2: (a) Position of the free solid. (b) Numerical and analytical friction coefficient relation.

3.2 3D dam breaking

To verify the contact-contact model in a case of high complexity, the model is applied to a case of free solid transport in free surface flow, modeled as a 3D experimental dam breaking event, which free cubic solids interact each other and fixed walls [6].

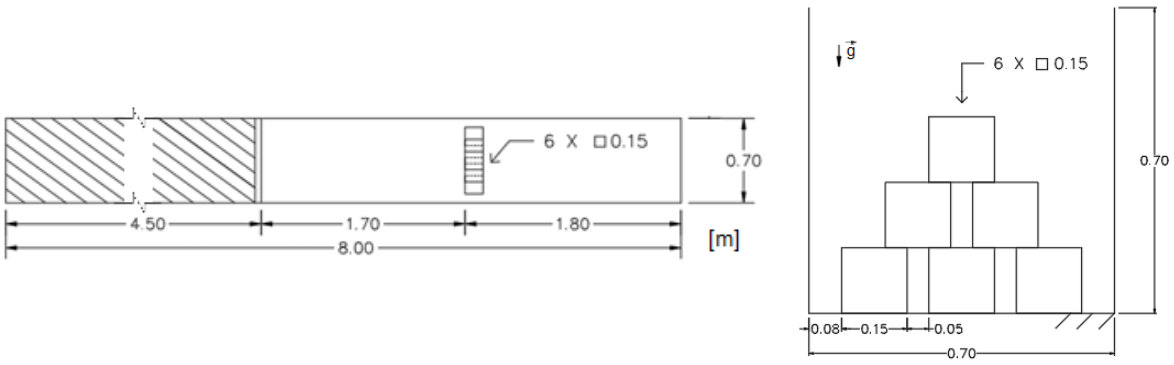

(a) (b)

Figure 3: (a) Main dimensions of the 3D dam breaking. (b) Triangular formation of cubes.

The experiment consists of a very long canal with dimensions 8.0 x 0.7 x 0.7 m³, a squared floodgate that holds water to the height of 0.4 m, installed at 4.50 m from the upstream wall, and 6 cubes of side 0.15 m arranged in a triangular formation. The cubes are placed 1.7 m away from the gate, where each cube is separated from its neighbor by 0.05 m. The central cube has its center of mass aligned with the central axis of the canal. Figure 3 shows the main dimensions of the geometry.

The floodgate ascends with a constant velocity of 1.9 m/s, to open completely in 0.21 s. The simulation is performed with time step $\Delta t = 5x10^{-4}s$, the coefficient of artificial

compressibility $\alpha = 10^{-8}$, the relaxation coefficient $\gamma = 0.05$ and free surface threshold values $\beta_1 = 0.97$ and $\delta_1 = 0.2$. The other parameters used can be observed in Table 2.

Table 2: 3D dam breaking. Numerical and materials properties.

Solid	*lo* (m)	*L/lo*	*ρ* (kg/m3)	*m* (kg)	*v*	*E* (GPa)	C_n (kg/s)	*μ*
Cube	0.0125	12	800	2.7	0.3	3	0.1	0.15
Wall		-	∞	∞	0.3	210	-	0.25

Figure 4 shows a sequence of frames from the experiment, simulations obtained by SPH [6], and the simulation carried in the present study. At the instant 0.95 s, the water front begins transporting the cubes downstream. The cubes at the base are transported by the water front while the remaining cubes fall at the instant 1.15 s. After this, all the cubes are carried by the wave front, although the cubes at the base present a delay in the motion computed by the present simulation compared to experimental results and simulation obtained by SPH method.

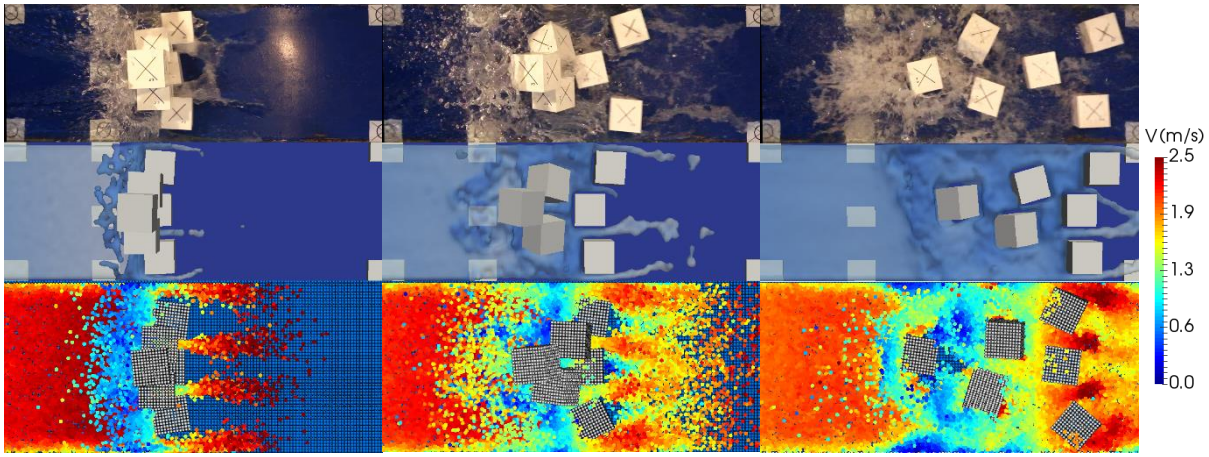

t = 0.95 s *t = 1.15 s* *t = 1.45 s*

Figure 4: Snapshots of the 3D dam breaking simulation. (top) Experiment, (middle) simulations obtained by SPH [6], and (bottom) the simulation carried in the present study.

The position of the center of mass of the cube at the top obtained by the present simulation, and experimental and numerical results are given in Figure 5. After the fluid hits the cubes at base, the cube at the top starts the motion along the longitudinal axis at the instant 0.85 s. The cube falls and is transported by wave front between the instants 1.07 and 1.40 s. Compared to experimental results, the cube presents a lower returning at the instant 1.30 s, and a faster fall between the instants 1.22 and 1.36 s. However, both computed motions along the x and z directions show a good agreement with experimental ones.

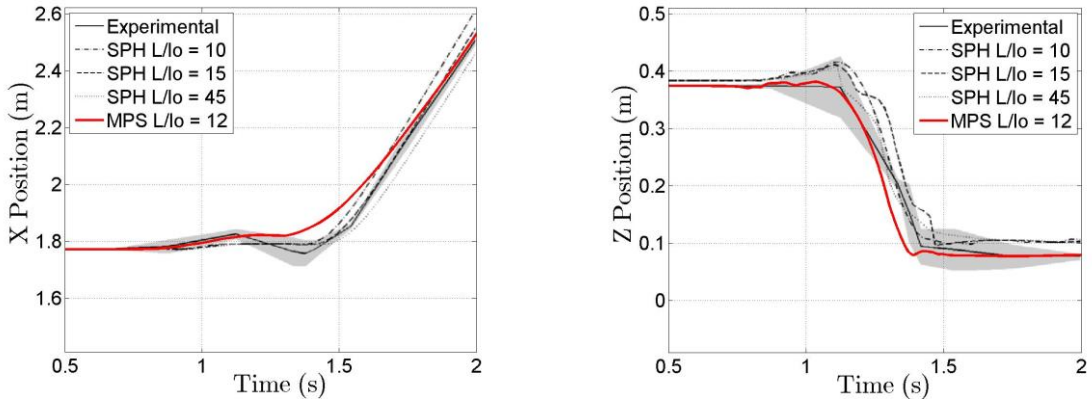

(a) (b)

Figure 5: Cube at the top. Motion along the (a) longitudinal and (b) vertical directions.

4 FINAL CONSIDERATIONS

A nonlinear spring and dashpot model for solid-solid contact and/or collision, based on contact mechanics theories, was investigated for Moving Particle Simulation (MPS) method in the present work. At first, the computed motion of a solid sliding on a sloped surface was compared to analytical motion, providing a linear relation between the numerical and analytical friction coefficients. After that, the model was applied to a case of solid transport in free surface flow, modeled as a dam breaking event with cubic solids interact each other and fixed walls. The positions of the solid obtained by the proposed model were compared with available numerical and experimental results. The comparisons of the results showed the effectiveness of the present approach to reproduce the main behaviors of free surface flow and multi-body interactions.

ACKNOWLEDGEMENTS

This work has financial support from CAPES and FDTE. The authors are grateful to Petrobras for financial support on the development of the MPS/TPN-USP simulation system based on MPS method.

REFERENCES

[1] Oh, S., Kim, Y. and Roh, B.S. Impulse-based rigid body interaction in SPH. *Computer Animation and Virtual Worlds* (2009) **20**:215-224.

[2] Amicarelli, A., Albano, R., Mirauda, D., Agate, G., Sole, A. and Guandalini, R. A Smoothed Particle Hydrodynamics model for 3D solid body transport in free surface flows. *Computers and Fluids* (2015) **37**:205-228.

[3] Harada, T., Tanaka, M., Koshizuka, S. and Kawaguchi, Y. Real-time coupling of fluids and rigid bodies. *In: APCOM 07 in conjunction with EPMESC XI* (2007).

[4] Ren, B., Jin, Z., Gao, R., Wang, Y.-X. and Xu, Z.-L. SPH–DEM modeling of the hydraulic stability of 2D blocks on a slope. *Journal of Waterway, Port, Coastal and Ocean Engineering*, **140** (2014).

[5] Asai, M. and Chandra, B. Numerical prediction of bridge wash-out during natural disaster by using a stabilized ISPH method. *In: Advances in Civil, Environmental and Materials Research* (2016).
[6] Canelas, R., Ferreira, R.M.L., Crespo, A.A.J.C. and Domínguez, J.M. A generalized SPH-DEM discretization for the modelling of complex multiphasic free surface flows. *In: 8th International SPHERIC Workshop* (2013).
[7] Koshizuka, S. and Oka, Y. Moving Particle Semi-implicit method for fragmentation of incompressible fluid. *Nuclear Science and Engineering* (1996) **123**:421-434.
[8] Tsukamoto, M.M., Cheng, L.-Y. and Nishimoto, K. Analytical and numerical study of the effects of an elastically-linked body on sloshing. Computers & Fluids (2011) **49**:1-21.
[9] Bellezi, C.A., Cheng, L.-Y. and Nishimoto, K. Particle based numerical analysis of green water on FPSO deck. *In: 32nd International Conference on Ocean, Offshore and Artic Engineering* (2013).
[10] Amaro Jr., R.A. and Cheng, L.-Y. Brittle fracture and hydroelastic simulations based on moving particle simulation. *Computer Modeling in Engineering & Sciences* (2013) **95**:87-118.
[11] Tsukamoto, M.M., Cheng, L.-Y. and Motezuki, F.K. Fluid interface detection technique based on neighborhood particles centroid deviation (NPCD) for particle methods. *International Journal for Numerical Methods in Fluids* (2016) **82**:148-168.
[12] Cundall, P.A. and Strack, O.D.L. A discrete numerical model for granular assemblies. *Geotechnique* (1979) **29**:47-65.
[13] Johnson, K.L. *Contact Mechanics*. Cambridge University Press, Cambridge (1985).
[14] Vetsch, D. *Numerical simulation of sediment transport with meshfree methods*. (Ph.D. thesis), ETH Zurich (2011).
[15] Hoomans, B. Granular dynamics of gas-solid two-phase flows. (Ph.D Thesis), University of Twente (2000).
[16] Coutinho, M.G. *Dynamic Simulations of Multibody Systems*. Springer-Verlag New York (2001).